MODELING CONDUCTIVITY AS A FUNCTION OF TEMPERATURE FOR CZTS AND CZTSe THIN FILM SOLAR CELL ABSORBER LAYERS

By

Melinda Downs

A Senior Honors Thesis Submitted to the Faculty of the University of Utah

In Partial Fulfillment of the Requirements for the

Honors Degree in Bachelor of Science

In

Materials Science and Engineering

Approved:

_____	_____
Dr. Michael Scarpulla	Dr. Feng Liu
Faculty Advisor, MSE	Department Chair, MSE
_____	_____
Professor David Richerson	Dr. Dinesh Shetty
Senior Thesis Advisor, MSE	Department Honors Advisor

_____

Dr. Sylvia D. Torti

Dean, Honors College

December 2013

ABSTRACT

The goal of this project was to develop an accurate model for the temperature dependent conductivity of Cu_2ZnSnS_4 (CZTS) and $Cu_2ZnSnSe_4$ (CZTSe) thin film solar cell absorber layers. Mathematical models of conductivity and resistivity were derived from both parallel and series combinations of temperature dependent charge carrier transport mechanisms. Specifically, this paper focuses on charge carrier transport associated with hopping, grain boundary, and freeze out mechanisms. These mechanisms were used to derive mathematical expressions to model conductivity as a function of temperature. The mathematical models were subsequently incorporated into a computer program, and the models tested against experimental data using non-linear fitting methods. Using these procedures, some models were eliminated and others shown to be more probable in giving a good description of the measured conductivity for CZTS and CZTSe absorber layers. The physics incorporated into the successful models helps give insight into the dominant transport processes in these thin films.

TABLE OF CONTENTS

INTRODUCTION

One source of renewable energy is the direct conversion of solar energy to electricity via solar cells, which is one of the fastest growing renewable energy technologies. As is true for any technology, there are advantages and disadvantages to solar energy and solar cells. One of the greatest current hindrances to the commercialization of solar cell technologies is that they are not quite as economically competitive when compared to common energy sources available, such as coal or natural gas. However, this argument does not take into account non-monetized effects such as the release of greenhouse gasses, particulate emissions, and the risk of spills associated with reliance on fossil fuels. For solar cells, there are two primary factors that must be balanced to achieve a competitive technology: cost and efficiency. The most common motivation for thin film solar cell research and development is that the use of less material and the ability to deposit thin films over large areas translates to the potential for lower manufacturing costs. Thin films also bring the possibility for less expensive substrates, a part which provides mechanical support and encapsulation of the active cell, which would act to lower manufacturing costs as well.

In addition to materials costs, the other major factor in cost evaluations is the processing requirements for solar cells. The easiest and least expensive techniques for fabricating thin films are generally borrowed from the electronics industry. These techniques most commonly produce polycrystalline films as the final product[1]. The importance of polycrystalline thin film solar cell materials as it relates to this study is that there are numerous electronic effects grain boundaries introduce to the thin film. Specifically, this paper focuses on charge carrier transport associated with hopping, grain boundary, and freeze out mechanisms.

Charge carrier transport mechanisms can be related to conductivity, a material property that describes the ability of the material to transfer charge (conduct electricity). Conductivity is inversely related to resistivity, a material specific factor incorporated in the resistance for the solar cell device.

Resistance can be related to the efficiency[2] by:

$$\eta = \frac{Jsc * Voc * FF}{Ps}$$

η = efficiency
Jsc = short circuit current density
Voc = open circuit voltage
FF = fill factor
P = incident light power density
V = voltage

$$V = I*R$$

R = resistance
I = current
V = voltage

Changes in resistance result in changes in voltage and/or current from Ohm's law (V=I*R), which then affect the Jsc, Voc, and FF in the efficiency equation for the solar cell device.

The efficiency, or ratio of electrical power produced to solar power incident on the cell, is one of the main limiting factors for solar cell commercialization currently. A significant focus of recent solar cell research and development has been in understanding electronic behavior of solar cell absorber layer materials and optimizing efficiency of solar cell devices. Clear understanding of the electronic behavior of the material will significantly improve the ability to optimize materials and processing, resulting in higher efficiencies for thin film solar cell devices. The approach taken in this paper is to increase comprehension of the electronic behavior associated with the resistivity and conductivity of the absorber layer material.

It should be noted that testing a working solar cell device versus the absorber layer alone is quite different. The difference is based on the depletion region, or the area near a pn junction where charge carriers have been completely removed due to the presence of an electric field and diffusion[2]. In a working device, which will be forward biased by the incident sunlight, the resistivity of this quasi-neutral region will contribute to series resistance and thus reduce the fill factor. The absorber layer alone will not have a depletion region. Therefore, testing the absorber layer alone will primarily focus on charge carrier transport outside of the depletion region[3]. Understanding transport in the regions outside of the depletion region is important for instances where the depletion region does not extend through the entire film[3].

The goal of this project was to develop an accurate model for the temperature dependent conductivity of Cu_2ZnSnS_4 (CZTS) and $Cu_2ZnSnSe_4$ (CZTSe) thin film solar cell absorber layers. Each model incorporates at least six free parameters, and each physical mechanism is predicted to have a different temperature dependence. Therefore, recording conductivity for a large number of temperatures can provide sufficient data to constrain the parameter values. Mathematical models of conductivity and resistivity were derived from both parallel and series combinations of temperature dependent charge carrier transport mechanisms. In the remainder of this paper the common charge carrier transport mechanisms for polycrystalline thin films are described, as well as their temperature dependence and relationships to each other. The

derivation of the mathematical expression is also illustrated, as well as the subsequent optimization to match experimental data using non-linear fitting methods.

BACKGROUND AND LITERATURE REVIEW

There are many materials currently being studied for thin film solar cells. The leading materials include amorphous silicon (a-Si), cadmium telluride (CdTe), copper indium gallium di-selenide (CIGSe), and organic molecules. While there has been a great deal of progress to higher efficiencies with these materials, there remain some cost considerations for commercialization. One consideration is that some of the raw materials have limited supplies and therefore are more expensive, as is true for tellurium and indium and to some degree selenium. The limited supply of some of these materials can also potentially act to increase production costs dramatically by overbalancing the supply and demand ratio for the raw materials. If the demand for the raw materials outstripped the supply due to sudden and large increases in use of the material due to mass production of these solar cells, raw material costs would again increase dramatically. This was seen in the period between 2004-2007, when the prices of silicon and indium both fluctuated by large amounts because of increased demand for new flat display technologies.

This study focused on thin film solar cell absorber layers made of copper zinc tin sulfide (Cu_2ZnSnS_4), better known as CZTS, and copper zinc tin selenide ($Cu_2ZnSnSe_4$),or CZTSe. Their advantage over more well known thin film solar cell materials lies in the fact that they are composed of commodity elements. These elements are both geologically abundant and mined in large quantities, or produced as byproducts of other major mining processes. Due to the current large supply capabilities mentioned for the raw materials of CZTS, technologies derived with CZTS would be able to avoid the supply and demand issue other solar cell materials would have to consider for mass production at greater than 100 gigawatts per year production levels.

Reducing the cost of manufacturing through material selection helps a great deal to further this technology along the road to commercialization. However, if the efficiency of the solar cell is not high enough, the cost per kilowatt hour of electricity over the 25+ year lifespan of the cells will still not be advantageous compared to other forms of energy, such as coal or natural gas. Efficiency in solar cell devices is a function of material properties, a very important one being conductivity. This and related concepts are explained in more detail in the following sections.

How a Solar Cell Works

The basis of a solar cell is the conversion of light to electricity via the photovoltaic effect. In the photovoltaic effect, incoming photons excite electrons from the valence band (where electrons are localized) of a semiconducting material to the conduction band (where electrons are free to move) leaving behind a "hole," or positive charge. The difference in energy between the conduction band and the valence band is referred to as the bandgap, and is material dependant.

The electrons and holes generated in the material due to the photovoltaic effect must be spatially separated rapidly to avoid recombination, which is where the electron falls back down and annihilates the hole. This results in a loss in current and/or voltage, which equates to a loss in efficiency for the device. There are three main types of recombination: non-radiative, radiative, and Auger. Non-radiative recombination is facilitated by characteristic material electronic defects which are typically associated with structural defects. Radiative and Auger recombination are intrinsic material properties however. Certain types of electronic defects can be studied via charge carrier transport phenomena, hence the importance of recognizing and understanding the active transport mechanisms in a specific material. Conductivity and resistivity are the material properties linked to charge carrier transport; better charge transport equates to higher conductivity and therefore lower resistivity for the material.

POLYCRYSTALLINE SEMICONDUCTORS

Central to the idea of polycrystalline materials is grains and grain boundary formation. Nuclei of forming grains cannot communicate with each other as they grow, leading to grains with various crystallographic orientations. Thus, when the grains grow to the point that they begin to impinge on their neighboring grains, the misalignment between the orientations of the grains necessitates defects in crystalline order along boundary between the grains. Such defects include dangling bonds, dislocations, interstitials, vacancies, distorted bond angles and bond distances, atoms in the wrong lattice sites, vacancies, and extrinsic impurities[4].

The mentioned types of physical defects in many cases create lower energy states located within the bandgap of the material, creating electron defects referred to as mid-gap states or trap states. Mid-gap states are able to trap electrons because the mid-gap states are at a lower energy and therefore more advantageous to occupy than the conduction band. The increased concentration of electrons in these states around grain boundaries can start to repel

other electrons, creating a potential barrier at the grain boundary as well as scattering effects that limit charge carrier mobility. In this way, grain boundary effects can be related to grain boundary transport mechanisms. This is of particular note for CZTS, due to the commonly seen compositional variance of copper (copper poor or copper rich) in CZTS absorber layers. This effect has been related to the formation of shallow dopant and deeper defect energy levels within grains and grain boundaries of CZTS[3].

Electronic Effects and Conductivity

The resistivity of a material links the material's properties and behavior to the efficiency of a solar cell through resistance and Ohm's law as previously stated. Due to the inverse relationship between resistivity and conductivity, an increase in resistivity reduces the conductivity for the device and leads to lower overall efficiency. Resistivity or conductivity versus temperature behavior of the material can be used to isolate various characteristic electronic phenomena. The conductivity versus temperature behavior of thin film materials can point toward charge carrier transport mechanisms that characterize the electronic behavior of the material in particular temperature regimes. CZTS in thin film solar cells is not as well characterized as it is for other thin film solar cell materials. Knowing which transport mechanisms dominate will help to further understand electronic device physics for CZTS thin film solar cells, and can eventually help determine methods of increasing efficiencies for these devices.

Resistivity can in general be considered a measure of charge carrier "resistance to motion" in the material. Conductivity on the other hand can be considered in a general sense to be a measure of the mobility of the same charge carriers. It follows that the "resistance to motion" for charge carriers is inversely proportional to the mobility. It is clear then that mobility describes the ability of charge carriers to travel within the material.

The mobility and "resistance to motion" for charge carriers are described in terms of the active mechanisms for the scattering of charge carriers in the material. The two main parameters used to characterize scattering phenomena in materials are the mean free scattering time (or mean time between collisions) and the mean free path (or the mean distance between scattering events)[5]. The mobility of charge carriers in a material is limited by the mechanism having the lowest scattering time. Commonly, for singe-crystalline semiconductor samples, the dominant mechanisms are lattice vibrations at high temperature and impurity

scattering below approximately 100K[5]. Grain boundaries introduce crystal defects, which will limit the mobility further. Therefore, grain boundary scattering is most likely a large player in highly polycrystalline samples[5]. This is of particular importance for this study, due to the polycrystalline nature of the CZTS samples being studied.

Conductivity in its most basic form is proportional to both the mobility (μ) and concentration (n, assuming electrons) of the charge carriers ($\sigma = ne\mu$). Both mobility and carrier concentration have temperature dependencies. As the temperature increases a material system has more energy, leading to increases in both the mobility as well as carrier concentrations, and therefore increasing the conductivity of the device. The temperature dependent behavior of the mobility and carrier concentration is then used as the basis for the temperature dependency for active carrier transport mechanisms within the material. In the following section, common charge carrier transport mechanisms for polycrystalline semiconductor thin films are discussed.

CHARGE CARRIER TRANSPORT MECHANISMS

As mentioned to above, defect states at grain boundaries may produce energy barriers which carriers must overcome in order to cross from grain to grain; this makes the mobility temperature dependent. It is important to note that this is not typically described in the same momentum scattering framework as is used for the mobility effects discussed above. Grain boundary effects are usually the limiting factor for mobility near room temperature, as the grain boundary electronic barriers may be many times the thermal energy available. In this study, the charge carrier transport mechanisms considered were focused on the primary categories of grain boundary effects, freeze out, and hopping. There are two main methods of carrier transport pertaining to overcoming potential barriers at grain boundaries: thermionic emission and tunneling. Thermionic emission will be discussed first.

Thermionic emission is always associated with a potential barrier, and it is the barrier height that is of most importance instead of the shape[6]. For thermionic emission to dominate charge carrier transport, the collision or drift diffusion process must be negligible in the barrier layer. This means that the barrier width must be narrower than the mean free path, and the diffusion current after it is injected over the barrier must not be the limiting factor. Therefore, only the carriers with energies above the potential barrier escape via this method[6]. Thermionic emission usually dominates from room temperature to approximately 150K[3].

This study considered three distinct cases of thermionic emission, each having different temperature dependences. The first, designated thermionic emission (1), is for the case of partially depleted grains and band bending, or the simple Seto model[7]. This is the most commonly used relationship (see below). This is not always the only factor determining the barrier, as bandgap changes at grain boundaries result in competing grain boundary thermionic emission models from different grain boundary state scenarios and doping in grains. From these situations two additional relationships can be identified, designated as thermionic emission (2) and thermionic emission (3) (see below). These three thermionic emission mechanisms can be difficult to distinguish however[8].

Thermionic emission (1):

$$\sigma = C * T^{-1/2} * \exp\left(-\frac{E}{kT}\right)$$

Thermionic emission (2):

$$\sigma = C * T^{-1} * \exp\left(-\frac{E}{kT}\right)$$

Thermionic emission (3):

$$\sigma = C * \exp\left(-\frac{E}{kT}\right)$$

Tunneling is a quantum-mechanical phenomenon. To illustrate the general concept of this transport mechanism, consider a charge carrier represented by its wave function. The wave function is not "trapped" by the potential barriers at grain boundaries, and can extend into and penetrate through the barrier[6]. This allows for transport of the charge carrier from one side to the other. Temperature assisted tunneling has the following temperature dependence:

$$\sigma = C * T^{-3/2} * \exp\left(-\frac{E}{kT}\right)$$

The next carrier transport mechanism considered is freeze out. Freeze out is altogether different than the mentioned grain boundary effects, as it primarily induces a change in carrier concentration as opposed to the mobility dependence of the previous transport mechanisms. Freeze out is associated with the reduction of available charge carriers, hence the carrier concentration dependence. As the temperature is decreased across the ionization temperature, the charge carrier donors and/or acceptors (from doping or impurities) in the material can no longer remain ionized and will take back their respective charges to become neutral[6]. This is

typically seen in a very narrow temperature regime in polycrystalline samples however, and can be difficult to determine[9]. Freeze out has the following temperature dependence[9]:

$$\sigma = C * T^{3/2} * \exp\left(-\frac{E}{kT}\right)$$

Hopping, in a very general sense, is the random motion of localized charge carriers resulting in conduction. This is opposed to the movement in delocalized band states for perfect crystals. The hopping charge carrier transport mechanisms are usually seen below 150K[3] in most materials, however, this depends on the degree of crystalline and chemical disorder present. Two main types of hopping transport were considered, and are discussed in the following paragraphs from highest to lowest temperature regime association.

Nearest neighbor hopping (NNH) mechanism explains impurity conduction in doped and compensation doped semiconductors[10]. This mechanism is thermally activated, and also employs a tunneling process. For example, consider an electron below the Fermi energy. In NNH, the electron on encountering a phonon can jump to the nearest empty center (nearby state above the Fermi energy). NNH is a particularly plausible transport mechanism in CZTS due to the large number of native defects present that can act as hopping centers[3]. NNH has a conductivity temperature dependence of the form:

$$\sigma = C * \exp\left(-\frac{E}{kT}\right)$$

Due to the thermally activated nature of NNH, this transport mechanism would not be the most frequent hopping process at very low temperatures. Mott variable range hopping (MVRH) was developed to fill that gap. This mechanism incorporates an optimum hopping distance, accounting for both the low activation energies for long hops and the prefactor introduced due to the tunneling processes involved with long hops[10]. This is the most common low temperature charge carrier transport mechanism seen in literature, usually around and below 80K[11]. The conductivity temperature dependence of this mechanism follows the form[12]:

$$\sigma = C * T^{-1/2} * \exp\left(-\frac{E}{kT^{1/4}}\right)$$

EXPERIMENTAL PROCEDURES

The following section details the development of a mathematical model for conductivity as a function of temperature. The thought process and assumptions incorporated in this effort are explained, as well as the utilization of a computer program for the non-linear fitting of the model to experimental data. The following is a summary of this section.

Expressions for conductivity were derived in terms of temperature dependent transport mechanisms. Subsequent optimization of the free parameters in the models was done to match the models to experimental data. The level of agreement between each model and experimental data was quantified in the goodness of fit for each model. This was accomplished using the simplex method of non-linear fitting in the Matlab computer program.

Experimental Data

The measurement technique employed for the measured conductivity data is a through thickness measurement on thin films[3]. The temperature was varied from approximately 30 to 300K. This temperature range was used because it correlates to the known previously mentioned transport mechanisms. Determining which of these mechanisms are active over the temperature range will indicate electronic effects and physical characteristics for the absorber material. These properties can then be used to understand the behavior of the absorber layer in a solar cell device at operating temperatures.

A total of four data sets were analyzed. Two data sets were for CZTSe and two were for CZTS. The following three of the four total samples[*] were formed via sputtering and varying subsequent annealing of stacks[3] with serial numbers: 56R4, 60R4, 70R2. This technique results in grains smaller than the film thickness. The M3356-22 data set[13] for CZTSe, on the other hand, was for a sample formed via a thermal evaporation technique, resulting in grains spanning the entire film thickness. Grain size and shape were determined within the works[3,13] referenced.

To simplify the derivation of the models, the transport mechanisms were considered in both a purely parallel equivalent circuit configuration and a purely series equivalent circuit configuration. Imbedded in the parallel configuration models is the assumption that the grains in the samples were sufficiently large enough to traverse the thickness of the film. This project focused on this set of models due to the through thickness measurement technique employed in taking the experimental data. However, to be thorough, conductivity models based on transport mechanisms in a series configuration were also formed and tested.

Mathematical Models of Resistivity versus Temperature

Twenty four base models were derived from varying combinations of the high temperature phenomena paired with the low temperature phenomena. The mechanisms incorporated in the base models were as follows: Mott variable range hopping (MVRH), nearest neighbor hopping (NNH), freeze out, tunneling, and thermionic emission. There are three thermionic emission temperature dependencies considered in this study. The mechanisms incorporated in each base model and their corresponding temperature dependencies (i.e. n and m exponent values) are as follows.

	Mechanisms						
	MVRH [n=-0.5 m=0.25]	NNH [n=0 m=1]	Freeze out [n=1.5 m=1]	Tunneling [n=-1.5 m=1]	Thermionic Emission (1) [n=-0.5 m=1]	Thermionic Emission (2) [n=-1 m=1]	Thermionic Emission (3) [n=0 m=1]
model 19							
model 20							
model 4							
model 6							
model 21							
model 33							
model 28							
model 34							
model 29							
model 5							
model 7							
model 22							
model 23							
model 8							
model 16							
model 18							
model 10							
model 12							
model 17							
model 24							
model 26							
model 25							
model 27							
model 11							

Table 1: Table of mathematical models by serial number, with the transport mechanisms used in each highlighted.

1. Model 4: MVRH, tunneling, thermionic emission (1)
   n=[-0.5 -1.5 -0.5]
   m=[0.25 1 1]

2. Model 5: MVRH, tunneling, freeze out
   n=[-0.5, -1.5, 1.5]
   m=[0.25, 1, 1]

3. Model 6: MVRH, thermionic emission (1), freeze out
   n=[-0.5, -0.5, 1.5]
   m=[0.25, 1, 1]

4. Model 7: MVRH, NNH, thermionic emission (1)
   n=[-0.5, 0, -0.5]
   m=[0.25, 1, 1]

5. Model 8: MVRH, NNH, tunneling
   n=[-0.5, 0, -1.5]
   m=[0.25, 1, 1]

6. Model 10: NNH, tunneling, thermionic emission (1)
   n=[0, -1.5, -0.5]
   m=[1, 1, 1]

7. Model 11: NNH, tunneling, freeze out
   n=[0 ,-1.5, 1.5]
   m=[1, 1, 1]

8. Model 12: NNH, thermionic emission (1), freeze out
   n=[0, -0.5, 1.5]
   m=[1, 1, 1]

9. Model 16: NNH, thermionic emission (1), thermionic emission (2)
   n=[0, -0.5, -1]
   m=[1, 1, 1]

10. Model 17: NNH, thermionic emission (2), thermionic emission (3)
    n=[0, -1, 0]
    m=[1, 1, 1]

11. Model 18: NNH, thermionic emission (1), thermionic emission (3)
    n=[0, -0.5, 0]
    m=[1, 1, 1]

12. Model 19: MVRH, thermionic emission (1), thermionic emission (2)
    n=[-0.5, -0.5, -1]
    m=[0.25, 1, 1]

13. Model 20: MVRH, thermionic emission (1), thermionic emission (3)
    n=[-0.5, -0.5, 0]
    m=[0.25, 1, 1]

14. Model 21: MVRH, thermionic emission (2), thermionic emission (3)
    n=[-0.5, -1, 0]
    m=[0.25, 1, 1]

15. Model 22: MVRH, NNH, thermionic emission (2)
    n=[-0.5, 0, -1]
    m=[0.25, 1, 1]

16. Model 23: MVRH, NNH, thermionic emission (3)
    n=[-0.5, 0, 0]
    m=[0.25, 1, 1]

17. Model 24: NNH, thermionic emission (2), tunneling
    n=[0, -1, -1.5]
    m=[1, 1, 1]

18. Model 25: NNH, thermionic emission (3), tunneling
    n=[0 , 0, -1.5]
    m=[1, 1, 1]

19. Model 26: NNH, thermionic emission (2), freeze out
    n=[0, -1, 1.5]
    m=[1, 1, 1]

20. Model 27: NNH, thermionic emission (3), freeze out
    n=[0 , 0, 1.5]
    m=[1, 1, 1]

21. Model 28: MVRH, thermionic emission (2), freeze out
    n=[-0.5, -1, 1.5]
    m=[0.25, 1, 1]

22. Model 29: MVRH, freeze out, thermionic emission (3)
    n=[-0.5, 1.5, 0]
    m=[0.25, 1, 1]

23. Model 33: MVRH, thermionic emission 2, tunneling
    n=[-0.5, -1, -1.5]
    m=[0.25, 1, 1]

24. Model 34: MVRH, thermionic emission (3), tunneling
    n=[-0.5, 0, -1.5]
    m=[0.25, 1, 1]

Each of these base models were then used to derive mathematical models in both a purely parallel configuration of mechanisms and a purely series configuration. The mathematical models used were kept as simple as possible to avoid having numerous and varying fitting parameters, in order to simplify the coding necessary in Matlab. Within each model the parameters that were varied to fit the model to the data were the overall constant (prefactor) and the activation energy (in the argument of the exponential term). As each mechanism has one of each, 6 total parameters were varied during the non-linear fitting. For the assumption of a parallel equivalent circuit, the formula derived for conductivity has the input from the three mechanisms adding inversely. For a series equivalent circuit model, the mechanisms add directly. The general formula utilized in this study for conductivity due to a parallel and series combination of transport mechanisms is shown below.

$$\sigma_{parallel} = \frac{1}{\frac{1}{C1 * T^{n1} * \exp\left(-\frac{E1}{kT^{m1}}\right)} + \frac{1}{C2 * T^{n2} * \exp\left(-\frac{E2}{kT^{m2}}\right)} + \frac{1}{C3 * T^{n3} * \exp\left(-\frac{E3}{kT^{m3}}\right)}}$$

$$\sigma_{series} = C1 * T^{n1} * \exp\left(-\frac{E1}{kT^{m1}}\right) + C2 * T^{n2} * \exp\left(-\frac{E2}{kT^{m2}}\right) + C3 * T^{n3} * \exp\left(-\frac{E3}{kT^{m3}}\right)$$

Model Comparison to Experimental Data

The models outlined above were written within a Matlab code to systematically fit each model to the experimental data using non-linear fitting techniques. The method for non-linear fitting utilized was the simplex method through the use of the Matlab built-in function fminsearch. To increase the chances of the function finding the global minimum instead of local minima, the initial values for the parameters and therefore the starting position for fminsearch were randomly varied over a range I deemed reasonable. The function fminsearch was then

asked to minimize the error and keep it if the resulting goodness of fit value was smaller than on the previous try. The progression of the Matlab code is detailed below.

1. Import Excel file containing the experimental temperature and resistivity data.
2. Using the same temperature values as the experimental data, and the initial prefactor and activation energy values, calculate conductivity and resistivity values for the model.
3. Calculate the degrees of freedom (DOF) as the number of data values minus the number of parameters.

```
DOF = max(size(T))-max(size(pars));
```

4. Calculate the goodness of fit (GOF) using the least squares method: Square the difference (relative error) between the measured and model values, and sum over all data points (temperature values). Divide by the degrees of freedom to arrive at GOF.

```
square_err = (1/DOF)* sum((((meas_sigma - trial_fit)./meas_sigma).^2));
```

5. Minimize the GOF value for the model by varying and refining the parameters in the model. This was accomplished within the Matlab program through the fminsearch function, which utilizes the simplex method of non-linear fitting.
6. Pick new initial parameter values. Pick a random value within the range of the conductivity values for the measured data set for each of the prefactors, and pick a random value between 0.001 and 1.5 eV for each the activation energies (1.5 eV is the bandgap for CZTS, and thus represents the maximum reasonable value). This randomness allows the model to avoid being trapped in local minima.
7. Repeat step 5.
8. Repeat step 6-7 300 times, each time determining if the GOF found is less than the previous: if so save the values found for the parameters and the GOF.
9. Plot the experimental data and the model together, using the best GOF and corresponding parameter values found in the previous step for the model. Conductivity was plotted as log(sigma), and the x-axis was 1/T in order to make Arrhenius plots.
10. Plot the three individual mechanisms with the experimental data, using the best fit parameter values (found is step 8) in the mechanisms. Conductivity was plotted as log(sigma), and the x-axis was 1/T (Arrhenius plot).
11. Save both plots.

12. Save the conductivity values for the model using the GOF and parameters from step 8 in an excel file (where each model will be saved to its own spreadsheet).
13. Save the GOF and parameters found in step 8 to an Excel file.
14. Repeat steps 2-13 for each of the 24 models.
15. Repeat steps 1-14 for each experimental data set (4 total).

DATA AND ANALYSIS

A number of additions were made to the Matlab code developed for non-linear fitting to enhance the overall accuracy of the modeling procedure. First, the mathematical models were modified by taking the absolute value of each of the six parameters that were used for fitting the model to experimental data (the prefactors and activation energies). This enabled the restriction of the Matlab fminsearch function to physically meaningful (i.e., non-negative) values.

Next, the code was modified to avoid the possibility of the fminsearch function being pulled into a local minimum. I addressed the issue of local minima by varying the starting guesses for each of the six parameters. For each model, after the initial fitting I created a loop where each initial guess (i.e., starting location) for each parameter was changed to a random number between a range of values. For the prefactors, I generated a random number between the maximum and minimum measured conductivity values. For the activation energies I generated values between 0.1meV and 1.5 eV (the bandgap of CZTS). Then these starting guesses were called back into fminsearch to be optimized again. This entire process was repeated 300 times for each model, and each time if the resulting values gave better GOF values they were stored such that after the loop the final parameters and GOF values should represent the best fit of that model to the experimental data possible (i.e., the global minimum of GOF within the six-dimensional function space for that model).

The entire operation for iterating through random starting locations for fitting the models to data described above was also repeated 5 times, as an added precaution. If the fitting function does actually find the global minimum, all five trials should be the same. See Appendix I for the finalized Matlab code.

The next stage was to ensure that the fitting function was matching the mechanisms in each model to the logical temperature range for that mechanism. This can be directly determined by comparing the activation energies assigned to each mechanism after being

fitted. Correct assignment of the mechanisms can also be qualitatively determined via the plots generated for each model of the separate mechanisms with the experimental data. Both of these methods were used to identify models that were correctly fitted as well as illustrate how the computer program was handling the mechanisms in each model.

Upon collecting the fitted parameter data I discovered that the computer program had assigned huge activation energies to one of the mechanisms in a few of the models on a number of the data sets. This effectively zeroes out that mechanism such that the function was essentially fitting a 2 mechanism model. This would be equivalent to saying that a 2 mechanism model fit better than a 3 mechanism model that included the zeroed mechanism. However, there should be 3 mechanisms for the most accurate fit, due to the nature of the data. This is best described by Arrhenius plots of the experimental data sets. When plotted as such, there are two linear sections (one for high temperatures and one for low temperatures) with a curved section joining them (see Figure 1).

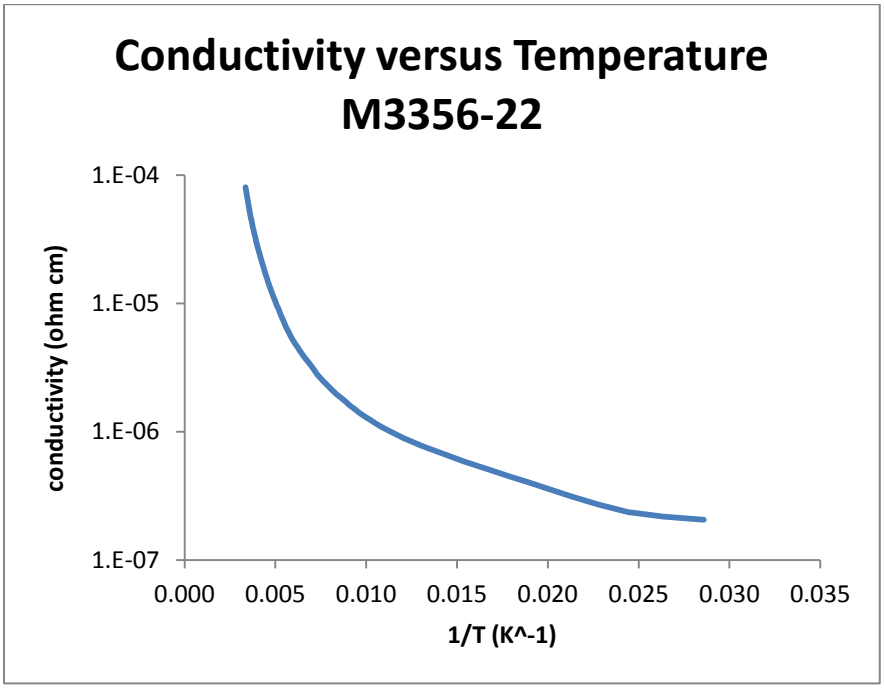

Figure 1: Arrhenius Plot of Conductivity versus Temperature for data set M3356-22.

In order to accurately account for the three distinct regions, the model requires three mechanisms. Therefore, the models that were fitted by zeroing a mechanism were deemed inaccurate and discarded. Such instances were recorded in the following tables. The series or parallel designation of each model is listed, along with the name of the zeroed mechanism and on which trials the mechanism was zeroed.

70R2 (CZTSe)			
Model Serial Number	**Parallel or Series**	**Mechanism**	**Trial**
model 4	parallel	MVRH	all trials
model 4	series	tunneling	trial 1 and 2
model 4	series	thermionic emission	trial 3-5
model 5	series	freeze out	all trials
model 6	series	freeze out	all trials
model 7	series	MVRH	all trials
model 8	series	tunneling	trial 1-3
model 10	series	tunneling	trial 3-5
model 12	series	freeze out	trial 3-5
model 16	series	thermionic emission 2	all trials
model 19	series	thermionic emission	trial 2 and 3
model 20	series	MVRH	trial 2-5
model 20	series	thermionic emission 3	trial 1
model 22	series	NNH or thermionic emission 3*	all trials
model 23	series	thermionic emission 2	trial 2
model 24	series	tunneling	trial 3-5
model 28	series	thermionic emission 2	trial 1
model 28	series	freeze out	trial 2-5
model 29	series	freeze out	all trials
model 33	series	tunneling	trial 1-3
model 33	series	thermionic emission 2	trial 4 and 5
model 34	series	tunneling	trial 1-3

Table 2: Models that when fitted had one mechanism zeroed out as seen in extremely large activation energy values for data set 70R2 (CZTSe). *Note that because NNH and thermionic emission (3) have the same temperature dependence the computer cannot tell them apart, and this model has both so either could be zeroed.

M3356 - 22 (CZTSe)			
Model Serial Number	**Parallel or Series**	**Mechanism**	**Trial**
model 4	parallel	MVRH	trial 3
model 5	series	tunneling	all trials
model 11	series	tunneling	trial 1-3
model 24	series	tunneling	trial 3-5
model 33	series	tunneling	all trials

Table 3: Models that when fitted had one mechanism zeroed out as seen in extremely large activation energy values for data set M3356-22 (CZTSe).

56R4 (CZTS)			
Model Serial Number	**Parallel or Series**	**Mechanism**	**Trial**
model 4	parallel	MVRH	all trials
model 4	series	tunneling	trial 1 and 2
model 5	series	tunneling	all trials
model 10	series	tunneling	all trials
model 24	series	thermionic emission 2	trial 2-4
model 24	series	tunneling	trial 1 and 5
model 33	series	tunneling	all trials

Table 4: Models that when fitted had one mechanism zeroed out as seen in extremely large activation energy values for data set 56R4 (CZTS).

60R4 (CZTS)			
Model Serial Number	**Parallel or Series**	**Mechanism**	**Trial**
model 4	parallel	MVRH	all trials
model 4	series	tunneling	trial 1
model 10	series	tunneling	trial 1-3
model 17	series	thermionic emission 2	trial 1
model 33	series	tunneling	all trials

Table 5: Models that when fitted had one mechanism zeroed out as seen in extremely large activation energy values for data set 60R4 (CZTS).

For all four data sets, the tunneling mechanism zeroed out most often in the models. For the CZTS data sets, the second most commonly zeroed mechanism was thermionic emission 2. For the CZTSe data sets, the second most commonly zeroed out mechanism was freeze out.

It should be noted that an important assumption in the computer code is that the order in which the mechanisms are input to the mathematical models does not matter; it should be able to match each mechanism to the correct temperature range regardless. However, this was not seen in the special case of models 21 and 22. The computer program should not be able to tell the difference between these two models, as the temperature dependency for NNH and thermionic emission (3) are identical and the other two mechanisms utilized in each model are the same. The same values should have been output for both of these models if it truly did not matter what order the mechanisms were in, but this was not the case for the GOF or fitted parameters.

Some inconsistency was also seen between the 5 trials for each model on each data set. Before implementing the FOR loop for different starting locations, multiple trials for fitting the models to experimental data gave varying answers for two of the three mechanisms between trials. After implementing the FOR loop, however, this was reduced to small variance in

parameter values for one mechanism in each model between trials. This indicates that while the addition of the FOR loop to iterate through different starting locations helped, it did not entirely enable the function to find the absolute bottom of the global minimum. It is possible that this is because there may not be a definitive global minimum to the parameter space the function is searching, due to the presence of large amounts of noise in the data sets. Particularly noisy data may even contain discontinuities and other troublesome features that would further decrease the ability of the computer program to determine a global minimum within the iterations specified in the computer code.

The final and ultimately most crucial boundary condition for the data is to determine whether mechanisms were matched to the correct temperature regime. Given the temperature dependencies and relationships of each of the mechanisms, the criteria are as follows for the fitted activation energy parameters: Hopping mechanisms should have lower activation energies than any of the other mechanisms, and MVRH should have smaller activation energies than NNH. Freeze out should have a lower activation energy than tunneling or any of the thermionic emissions. Tunneling should have lower activation energies than the thermionic emissions as well, leaving the thermionic emission mechanisms with the highest activation energies.

The previous boundary conditions were then used to determine whether the model was correctly fitted to the experimental data. This was done by systematically checking the activation energy values assigned for each mechanism in each model on all four data sets. Below is the tabulated goodness of fit (GOF) data for all data and models. GOF values highlighted in red are for those models that passed all of the boundary conditions discussed above. Bolded entries represent the best (i.e., smallest) GOF for that particular data set.

	CZTS GOF			
	parallel		**series**	
	56R4	**60R4**	**56R4**	**60R4**
model 4	**0.0953**	**0.1152**	0.0068	0.0216
model 5	0.1022	0.1162	0.0104	0.0203
model 6	0.2427	0.1604	0.0013	0.0026
model 7	0.2188	0.2268	0.0012	0.0039
model 8	0.1170	**0.1151**	0.0044	0.0205
model 10	0.2290	0.2807	0.0292	0.0360
model 11	0.2257	0.2808	0.0039	0.0081
model 12	0.1911	0.2267	0.0029	0.0037
model 16	0.2523	0.2630	0.0259	0.0186

	CZTSe GOF			
	parallel		**series**	
	70R2	**M-22**	**70R2**	**M-22**
model 4	0.0227	0.1711	2.50E-05	5.57E-03
model 5	0.0006	0.1586	2.50E-05	4.11E-03
model 6	0.0002	0.2833	3.39E-05	9.48E-04
model 7	0.0002	0.2717	2.77E-05	5.08E-04
model 8	0.0004	**0.1500**	6.55E-05	1.85E-03
model 10	0.0159	0.3137	2.77E-05	7.50E-03
model 11	0.0043	0.3136	5.85E-04	4.62E-03
model 12	0.0017	0.2640	2.77E-05	1.05E-03
model 16	0.0190	0.2999	2.77E-05	1.26E-02

model 17	0.2641	0.2644	0.0201	0.0328
model 18	0.2188	0.2299	0.0170	0.0143
model 19	0.2488	0.2627	0.0038	0.0137
model 20	0.2313	0.2464	0.0014	0.0059
model 21	0.2186	0.2541	0.0014	0.0042
model 22	0.1664	0.1156	0.0014	0.0042
model 23	0.2186	0.2267	**0.0010**	0.0029
model 24	0.2398	0.2806	0.0322	0.0380
model 25	0.2613	0.2809	0.0121	0.0222
model 26	0.2386	0.2385	0.0026	0.0045
model 27	0.1510	0.1597	**0.0010**	0.0031
model 28	**0.0951**	0.1172	0.0014	0.0037
model 29	0.1716	0.2267	0.0011	**0.0022**
model 33	0.0968	0.2791	0.0123	0.0276
model 34	0.0960	0.1156	0.0029	0.0131

model 17	0.0208	0.2656	7.09E-05	6.79E-03
model 18	0.0071	0.2694	2.77E-05	1.11E-02
model 19	**0.0001**	0.1523	2.80E-05	1.03E-03
model 20	0.0002	0.2640	2.77E-05	5.08E-04
model 21	0.0002	0.1502	3.48E-05	**4.77E-04**
model 22	**0.0001**	0.1509	2.80E-05	**4.80E-04**
model 23	0.0002	0.2640	6.55E-05	7.15E-04
model 24	0.0225	0.3066	2.08E-05	1.50E-02
model 25	0.0113	0.3154	7.09E-05	1.13E-02
model 26	0.0038	0.2640	5.69E-04	1.40E-03
model 27	0.0004	0.1954	7.09E-05	8.64E-04
model 28	**0.0001**	**0.1499**	2.80E-05	9.32E-04
model 29	0.0002	0.2640	6.55E-05	1.92E-03
model 33	0.0007	0.1511	2.80E-05	6.43E-03
model 34	0.0003	0.1500	6.55E-05	2.95E-03

Tables 6: GOF values for each model (series and parallel) on each CZTS data set. Table 7: GOF values for each model (series and parallel) on each CZTSe data set. Highlighted values are for models that passed the boundary conditions.

First, compare the parallel based models on the CZTS data sets 56R4 and 60R4. Of these, model 7, model 16, model 21, and model 25 were consistently correctly fitted to the experimental data for both the CZTS data sets. From related studies of CZTS[3] the parallel configuration of model 7 was expected to do the best. While the parallel based model 7 did in fact work for the CZTS data sets, it is debatable whether it did the best of all the models that met the boundary conditions. None of the series based models, however, showed consistently correct fitting to experimental data for both CZTS data sets.

Comparison of the parallel configuration based models for the CZTSe data sets (70R2, M3356-22) yielded similar results. Of the parallel based models only model 10, model 16, model 18, and model 26 were consistently correctly fitted to the experimental data for both CZTSe data sets. None of the series based models showed consistently correct fitting to experimental data for both data sets for CZTSe as well. It is interesting that of all the models, only parallel model 16 was correctly fitted to experimental data for all four data sets.

The trend seen in the above data (Table 6) is that the parallel configuration based conductivity models did not match the data as well as the series configuration based conductivity models. This was visually corroborated in the plots of the experimental with the optimized models (see Figure 2). Note that the parallel based models when plotted compared to the experimental data show a different curve behavior than the series based models.

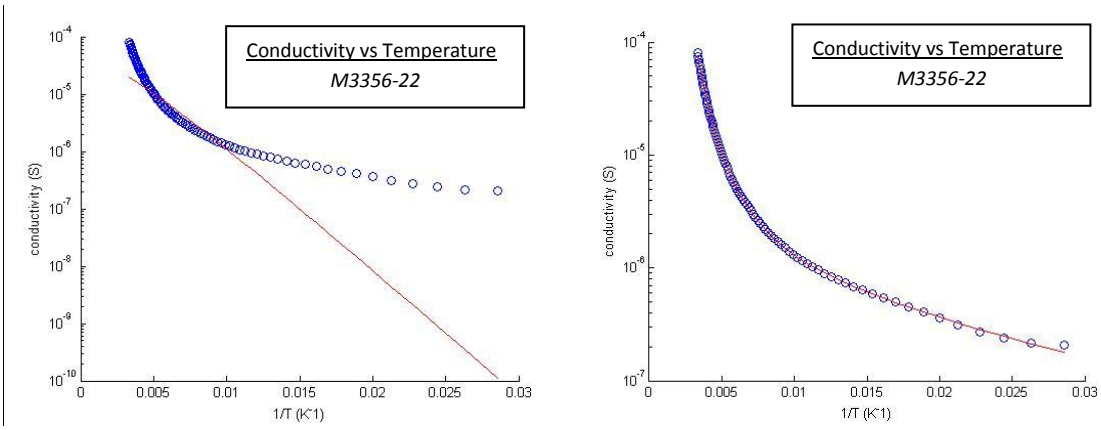

Figure 2: Representative plots of M3356-22 experimental data with fitted model 7. Left: parallel model 7. Right: series model 7.

Returning to the trend of series based models matching experimental data better than the parallel based models as supported by the GOF data, there are a number of other observations to be made in the data in Tables 6 and 7. First, most of the series configuration based models failed the activation energy boundary condition on all the data sets, while more of the parallel models did not. It is possible that the series configuration based models were able to fit the data better simply because of this lack of adherence to the activation energy boundary condition, and is a function of how the computer program operates. It is also possible that the series configuration based models fit better because of dominating series behavior. This could occur with conductivity behavior following a combination series and parallel equivalent circuit configuration, where the mechanism(s) in series are dominating those in parallel. The mechanism(s) in series could be dominating to the point where the computer program cannot distinguish the rest, also potentially explaining the lower ability of the computer program to match mechanisms in a purely series configuration correctly.

This series and parallel combination configuration actually makes more sense with the physical grain structure for the data sets 56R4, 60R4, and 70R2, where the grains are smaller than the film thickness. In this case, based on the through film measurements utilized in this study, you would expect the parallel equivalent circuit configuration within the grains. However, because the grains are smaller than the thickness, you then have to cross a grain boundary, creating a situation where the grain boundary mechanism(s) utilized to cross the grain boundary is in series with whatever mechanism(s) was used within the grain previously. Hence, it is expected that these samples show conductivity behavior based on a combination of mechanisms in series and parallel. This combination configuration makes much less sense the M3356-22 data, as based on Scanning Electron Microscopy images[12] the grains in this sample

span the thickness of the film (closely matching the purely parallel configuration assumption used for the parallel configuration based models). However, the same situation of better GOF values for all the series based models as opposed to the parallel based models seen for the other three data sets was also true for the M3356-22 data set, which as stated should be closest to mimicking the conditions of the parallel configuration assumption and should not show the same messy behavior as the other data sets.

CONCLUSION

It was expected that matching purely parallel or purely series configuration based models to the data sets for samples made via sputtering and annealing (grains smaller than the film thickness) would be less accurate. The most logical explanation for the samples prepared via sputtering and annealing techniques (56R4, 60R4, 70R2) is that the conductivity behavior follows a series and parallel combination equivalent circuit configuration, with the series mechanism(s) dominating. This is based on the understanding of the physical structure for these samples, where the presence of grains smaller than the film thickness indicate this type of behavior is likely. The dominating series mechanism(s) would be grain boundary effects. This physical grain structure also does not match the assumption made to create the purely parallel configuration based models, and the measurement technique employed does not indicate a series equivalent circuit configuration. Based on the measurement technique employed, all the series models also should not have done well, and proved to have the best GOF values for all models on all data sets. However, more series based models were incorrectly matched to the experimental data than parallel based models using the activation energy boundary conditions.

On the other hand, the M3356-22 experimental data set should have done well with the parallel configuration based models, as its physical grain structure is such that it matches the assumption of grains long enough to traverse the thickness utilized in this modeling configuration. This was not the case, as the parameter and GOF fit data for this data set failed to noticeably distinguish itself from the trends illustrated in the other three data sets. The series and parallel combination configuration theory does not seem nearly as likely for this data set assuming that the grains truly do traverse the thickness of the film. If perhaps a very thin layer formed underneath the long grains, the series and parallel combination behavior explanation would be much more reasonable for the M3356-22 data set.

Due to this outcome, in future studies it would be helpful to eliminate the purely parallel configuration or purely series configuration assumption that was used to derive the mathematical models. This could be accomplished by creating mathematical models based on series and parallel combination configurations. It would also be interesting to try more data sets for samples theoretically matching the long grain assumption, along with trying series based models on data taken via a cross film measurement technique. Data taken in this way should indicate a series equivalent circuit configuration, and so the series based models should be best able to describe the conductivity behavior. Comparing results from the described experiment to the ones found in this study could aid understanding of the series and parallel equivalent circuit configuration conundrum I encountered.

Future work could also focus on further refining of the computer code as well. Restriction of the parameter space in the function fminsearch to positive values, as opposed to forcing logical answers via the absolute value could help to speed up the computer program. Within the mathematical models, accounting for domain effects could also help increase accuracy. The computer code should also be refined to the point that there is high certainty in its ability to find the global minimum, and little to no variance in the parameters from different trials of fitting the same model to the experimental data. Once this has been accomplished, the prefactor values can be used to derive quantities such as the effective mass, bandgap, Fermi energy, and of course mobility and carrier concentration values. These would provide valuable information on the materials electronic structure as well as its unique electronic behavior, furthering our ability to hone in on effective techniques for increasing efficiencies for solar cells using CZTS and CZTSe materials.

Ultimately, the derivation of mathematical models for conductivity as a function of temperature was accomplished, as well as the creation of a Matlab computer code to match these models to experimental data using non-linear fitting techniques. While the Matlab code could be further tweaked to increase accuracy and efficiency, it provides a method of determining the ability of each mathematical model to describe the conductivity behavior seen in a given experimental data set, as well as indicating the dominating charge carrier transport mechanisms in the material over specific temperature ranges. When the mathematical models were tested against four experimental data sets, two each for CZTS and CZTSe, it was discovered that the assumption of purely parallel or purely series equivalent circuit configurations used in the creation of the mathematical models was inaccurate for all the data sets. This was expected

for three of the data sets corresponding to samples made via sputtering and annealing techniques; however, this is not what was expected for the sample made via a thermal evaporation technique. Future research into the best method of mathematically describing the way that the charge carrier transport mechanisms interact would be very useful in furthering our understanding of the conductivity behavior for CZTS and CZTSe thin film solar cell absorber layers.

ACKNOWLEDGEMENTS

I would like to thank Dr. Scarpulla, Volodymyr Kosyak and Mak Karmarkar for allowing access to their data sets, and Chris Dances and Matt Hamilton for Matlab debugging help.

REFERENCES

1. C. Grovenor, "Grain Boundaries in Semiconductors", *J. Phys. C.*, **18** 4079-4119 (1985).
2. J. Nelson, *The Physics of Solar Cells*. Imperial College Press, London, UK, 2003.
3. V. Kosyak, M. Karmarkar, M. Scarpulla, "Temperature Dependent Conductivity of Polycrystalline Cu2ZnSnS4 Thin Films", Appl. Phys. Lett., **100** 263903 (2012); doi: 10.1063/1.4731875.
4. C. Seager, "Grain Boundaries in Polycrystalline Silicon", Ann. Rev. Mter. Sci., **15** 271-302 (1985).
5. S. Kasap, *Priniciples of Electronic Materials and Devices*, 3rd ed.; McGraw-Hill, New York, NY, 2006.
6. S. SZE, K. Ng, *The Physics of Semiconductor Devices,* 3rd ed.; Wiley & Sons, Hoboken, NJ, 2007.
7. J. Seto, "The Electrical Properties of Polycrystalline Silicon Films", J. Appl. Phys., **46**, 5247 (1975).
8. G. Baccarani, B. Ricco, G. Spadini, "Transport Properties of Polycrystalline Silicon Films", Appl. Phys. Lett., **49**, 5565 (1978); doi: 10.1063/1.324477.
9. O. Gunawan et al., "Electronic Properties of the Cu2ZnSn(Se,S)4 Absorber Layer in Solar Cells as Revealed by Admittance Spectroscopy and Related Methods", Appl. Phys. Lett., **100** 253905 (2012); doi: 10.1063/1.4729751.
10. N. Mott, *Conduction in Non-Crystalline Materials*, 2nd ed.; Oxford University Press, New York, 1993.
11. C. Lien, C. Wu, Z. Li, J. Lin, "Electrical Conduction Processes in ZnO In a Wide Temperature Range 20-500 K", J. Appl. Phys., **110** 063706 (2011); doi: 10.1063/1.3638120.
12. N. Mott, E. Davis, "Electronic Processes in Non-Crystalline Materials", Science, **176** [4039] 1117 (1972).
13. I. Repins et al., "Co-Evaporated Cu2ZnSnSe4 Films and Devices", Solar Energy Materials and Solar Cells (2012); doi:10.1016/j.solmat.2012.01.008.
14. R. Bube, "Electronic Transport in Polycrystalline Films", Annu. Rev. Mat. Sci., **5** 201-224 (1975).
15. N. Lu et al., " A Conduction Model for Semiconductor-Grain-Boundary-Semiconductor Barriers in Polycrystalliine-Silicon Films", IEEE, transaction of Electron Devices, **30** [2] 137-149 (1983).

16. L. P. Scheller, N. Nickel, “Charge Transport in Polycrystalline Silicon Thin-Films on Glass Substrates”, J. appl. Phys., **112** 013713 (2012); doi: 10.1063/1.4733699.
17. D. Joshi, R. Srivastava, “A Model of Electrical Conduction in Polycrystalline Silicon”, IEEE, Transactions on Electron Devices, **31** [7] (1984).
18. M. Ada-Hanifi et al., “A Model of Conduction in Polycrystalline Silicon Films”, J. Appl. Phys., **62** [5] (1987).
19. M. Alt, H. Lewerenz, R. Scheer, “Influence of the Cooling Rate on the Electrical Conductivity of Coevaporated CuInS2 Thin Films”, J. Appl. Phys. **81** [8] 3667-3669 (1997).
20. B. Gunning et al., “Negligible Carrier Freeze-out Facilitated by Impurity Band Conduction in Highly N-type GaN”, Appl. Phys. Lett., **101** 082106 (2012); doi: 10.1063/1.4747466.
21. R. Punia et al., “Temperature and Frequency Dependent Conductivity of Bismuth Zinc Vanadate Semiconducting Glassy System”, J. Appl. Phys., **112** 083701 (2012); doi: 10.1063/1.4759356.
22. A. Amara et al., “Electrical and Optical Characterization of CuInS2 Crystals and Polycrystalline Co-evaporated Thin Films”, Solar Energy Materials and Solar Cells, **91** 1916-1921 (2007).
23. D.C. Look et al., “Deepcenter Hopping Conduction in GaN”, J. Appl. Phys., **80** 2960 (1996); doi: 10.1063/1.363128.
24. K. Chopra, *Thin Film Solar Cells*, Plenum Press, New York, 1983.

APPENDIX I

```
function [] = conductivity_fitting_3mech_300iter
clear, clc

global T
global meas_sigma

%load the measured data file
[fname,pname] = uigetfile('*.xlsx','Select the raw data file');
%select an excel file

%root_length = size(fname,2) - 4; %this takes the filename and strips
the ".dat" extension
%name_root = fname(1:root_length);

data = xlsread(strcat(fname)); %ignores headers and outer rows or
columns already, reads from first spreadsheet

% T = 1./data(:,1);    %this assumes the first column of a data file is
1/T.  Change if necessary.
T = data(:,1);    %this assumes the first column of a data file is T.
Change if necessary.

meas_sigma= data(:,2); %assumes list of conductivity values is in
second column of data file (and only one list of values)

[p,q]=size(meas_sigma);

%%%%%%%%%%%%%%%%% end data loading %%%%%%%%%%%%%%%

%%%%%%%%%%%%%%%%%%%% main calculation %%%%%%%%%%%%%%%%%%%%%%%

% the first number must equal the number of parameters being fit.
pars_save = zeros(q,6);
fit_save = zeros(p,q);
err_save = zeros(q,1);

%max limit number evaluations in fminsearch to 1e6
options = optimset('MaxFunEvals',1e9);

    %initial guesses pars(1)=C(1) pars(2)=C(2) etc.
    pars(1) = 0.1; % constant1
    pars(2) = 0.1; %constant2
    pars(3) = 0.1; %constant3
    pars(4) = 0.3; %energy1
    pars(5) = 0.5; %energy2
    pars(6) = 0.7; %energy3

    pars = [pars(1) pars(2) pars(3) pars(4) pars(5) pars(6)];

    %minimize GOF by varying pars,store new values of pars as pars
    pars = fminsearch(@square_err,pars,options);
```

```
%vary pars and try again, avoid local minima
best_pars = pars;  %this holds the best values of pars that you have
found so far.  We will update it in the loop if err^2 is better
best_err2 = square_err(pars);
Egap = 1.5;
min_data=min(meas_sigma);
max_data=max(meas_sigma);

for a=1:5
    for i=1:300    %pick some number here (change to while loop if
still doesn't work)

pars = [(min_data + (max_data-min_data).*rand(1)) (min_data +
(max_data-min_data).*rand(1)) (min_data + (max_data-min_data).*rand(1))
(0.1e-3+(Egap-0.1e-3).*rand(1)) (0.1e-3+(Egap-0.1e-3).*rand(1)) (0.1e-
3+(Egap-0.1e-3).*rand(1))];

pars = fminsearch(@square_err,pars,options);
square_error = square_err(pars);

if square_error<best_err2
best_pars = pars;   %now we hold onto only the best set of pars that
the loop finds
best_err2 = square_error;
end

end

pars = best_pars;  %this reassigns pars to the values found within the
loop
trial_fit = conductivityparallel_7(pars,T);  %this generates the best
model and GOF for those pars.
square_error = best_err2;

%collect final pars values and model fit data (conductivity values,GOF)
    pars_save = pars(:);
    fit_save = trial_fit;
    err_save = square_error;

    kB= 8.6173324e-5;
    Z=length(pars)/2;
    C=pars(1:Z);
    E=pars(Z+1:Z*2);
    prefactor = [-1.5 -1 -0.5 0 0.5 1.5];
    n=[prefactor(3) prefactor(4) prefactor(3)];
    expfactor=[0 1 0.25];
    m=[expfactor(3) expfactor(2) expfactor(2)];

    mech1=(abs(C(1)).*(T.^n(1)).*exp(-(abs(E(1))./(kB*(T.^m(1))))));
    mech2=(abs(C(2)).*(T.^n(2)).*exp(-(abs(E(2))./(kB*(T.^m(2))))));
    mech3=(abs(C(3)).*(T.^n(3)).*exp(-(abs(E(3))./(kB*(T.^m(3))))));

    %%%%%% plot experimental and fit model together vs (1/T)%%%%%%%

    B=figure(3);
```

```
    X=1./T;
    clf
    hold on
    plot(X, meas_sigma,'bo')
    plot(X,trial_fit,'r-')
    set(gca,'Yscale','log')
    xlabel('1/T (K^-1)')
    ylabel('conductivity (S)')
    hold off

    V=figure(4);
    clf
    hold on
    plot(X,meas_sigma,'ko')
    plot(X,mech1,'g-')
    plot(X,mech2,'r-')
    plot(X,mech3,'b-')
    set(gca,'Yscale','log')
    xlabel('1/T (K^-1)')
    ylabel(' log(conductivity) (S)')
    hold off

%%%%%%%%% Save All Data %%%%%%%%%%%%
name3=sprintf('posterplot_M-22_totalALT_CP_7c_I300_%d',a);
name4 = sprintf('posterplot_M-22_mechfitALT_CP_7c_I300_%d',a);

% Save Figures
saveas(B,name3,'jpg');
saveas(V,name4,'jpg');

% These save a separate file for the fitted model conductivity values
and the table of fit values (pars and GOF)
sheet2=sprintf('CP_7_I300_%d', a);
SUCCESS=xlswrite('MKCZTS70R2_CP_modelfitsAUTOTRIAL.xls',fit_save,sheet2
);
data2=[pars_save;err_save];
SUCCESS=xlswrite('MKCZTS70R2_CP_parsGOFfitAUTOTRIAL.xls',data2,sheet2);

end

display finished

%%%%%%%%%% Subroutines %%%%%%%%%%%%%%%

function [square_err] = square_err(pars)
global meas_sigma
global T

DOF = max(size(T))-max(size(pars));

[trial_fit] = conductivityparallel_7(pars,T);
square_err = (1/DOF)* sum((((meas_sigma - trial_fit)./meas_sigma).^2));
```

Name of Candidate:	Melinda Downs
Birth Date:	April 11, 1991
Birth Place:	Salt Lake City, Utah
Address:	15370 S 1800 W Bluffdale, UT 84065